Cu-Doped ZnO Nanoneedles and Nanonails: Morphological Evolution and Physical Properties

ARTICLE *in* THE JOURNAL OF PHYSICAL CHEMISTRY C · JUNE 2008

Impact Factor: 4.77 · DOI: 10.1021/jp710837h

THE JOURNAL OF PHYSICAL CHEMISTRY C

Article

Cu-Doped ZnO Nanoneedles and Nanonails: Morphological Evolution and Physical Properties

Zhou Zhang, Jia Bao Yi, Jun Ding, Lai Mun Wong, Hwee Leng Seng, Shi Jie Wang, Jun Guang Tao, Gong Ping Li, Guo Zhong Xing, Tze Chien Sum, Cheng Hon Alfred Huan, and Tom Wu

J. Phys. Chem. C, **2008**, 112 (26), 9579-9585 • DOI: 10.1021/jp710837h • Publication Date (Web): 07 June 2008

Cu-Doped ZnO Nanoneedles and Nanonails: Morphological Evolution and Physical Properties

Zhou Zhang,[†] Jia Bao Yi,[‡] Jun Ding,[‡] Lai Mun Wong,[§] Hwee Leng Seng,[§] Shi Jie Wang,[§] Jun Guang Tao,[†] Gong Ping Li,[†] Guo Zhong Xing,[†] Tze Chien Sum,[†] Cheng Hon Alfred Huan,[†] and Tom Wu*[,†]

Division of Physics and Applied Physics, School of Physical and Mathematical Sciences, Nanyang Technological University, Singapore 637371, Department of Materials Science and Engineering, National University of Singapore, Singapore 119260, Institute of Materials Research and Engineering, 3 Research Link, Singapore 117602

Received: November 13, 2007; Revised Manuscript Received: February 21, 2008

Controlling novel morphologies and developing effective doping strategies are two important tasks for advancing ZnO-based nanomaterials. We have grown vertically aligned Cu-doped ZnO nanonails and nanoneedles and observed a continuous evolution between various morphologies. Selecting source compositions and regulating vapor and gas pressures modify the Ehrlich−Schwoebel energy barrier for the surface diffusion and determine the morphologies. X-ray diffraction study indicates a decrease in the lattice parameter after the Cu doping. Photoluminescence measurements taken on both doped and undoped samples show that, in the Cu-doped ZnO nanostructures, the band-edge UV emission and the broad green emission are red-shifted by ∼7 and 20 nm, respectively. X-ray photoelectron spectroscopy study revealed a higher level of oxygen vacancies in nanoneedles, which was found to enhance the green emission. Room-temperature ferromagnetism was also observed in Cu-doped ZnO nanomaterials. On the basis of the strong correlations between structures and properties, we demonstrate that the morphologies and the optical and magnetic characteristics can be tailored to a large degree in transition-metal-doped ZnO nanostructures.

Introduction

Zinc oxide (ZnO) is one of the most important and versatile semiconductors with a direct wide band gap of 3.37 eV at room temperature.[1] Its strong exciton binding energy of 60 meV makes it very attractive for exciton-based lasing applications. ZnO has also great potential in applications in solar cells,[2] sensors,[3] photocatalysis,[4] transparent thin film transistors,[5,6] and so forth. Recently, extensive progress has been made on the research front of ZnO-based nanomaterials motivated by both basic sciences and potential advanced technologies.[7] Compared with their bulk and thin film counterparts, the one-dimensional morphology and the high surface-to-volume ratio intrinsic to nanomaterials often bring about novel properties. Indeed, ZnO nanostructures exhibit promising performances as field effect transistors, [8] UV photodetectors,[9] gas sensors,[10] field emission electron sources,[11] nanowire nanolasers,[12] nanoscale power generators,[13] and many other functional devices.

Several physical and chemical synthesis methods have been developed to synthesize ZnO based nanomaterials with tailored morphologies and properties.[14] The vapor−liquid−solid (VLS) process is widely adapted as the mechanism for growing one-dimensional structures, such as nanowires and nanorods.[15–17] In this process, the Zn vapor forms liquid-phase eutectic alloys with the catalytical particles and then condenses out as ZnO nanowires after reaching the supersaturation level. The disadvantage of the VLS route is that the catalyst often diffuses into the ZnO matrix during growth, creating deep traps within the band gap. On the other hand, the vapor−solid (VS) route requires no catalyst and appears to be more versatile.[18,19] Because the VS growth is not defined by the catalyst nanoparticles, a wide range of fascinating nanostructures have been produced, such as tetrapots, nanotubes, nanonails, nanohelices, nanorings, nanodisks, nanoneedles, nanocombs, and so forth.[7] It is noteworthy that many of these hierarchical nanostructures are created using a simple template-free vapor transport method. However, the formation mechanisms could be quite complex and often involves correlated factors such as intrinsic surface polarity, defect propagation, surface-dependent oxidation, and orientation-dependent growth speed.[20–23]

Herein, we report the synthesis of Cu-doped ZnO nanostructures that exhibit a continuous morphological evolution between nanoneedles and nanonails. With most of the previous works concentrating on undoped ZnO, there have been more and more efforts devoted to investigate the doped counterparts.[24–30] For semiconductors, doping is a powerful tool to tailor the electrical and optical properties, facilitating the construction of many electronic and optoelectronic devices. Cu doping modifies the photoluminescent (PL) transitions in ZnO by creating localized impurity levels.[31] Additionally, Cu behaves as an acceptor in ZnO with its energy level locating at 0.17 eV below the bottom of the conduction band, making itself a good candidate for creating *p*-type ZnO.[32] More interestingly, previous studies, both theoretical and experimental, showed that ZnO doped with appropriate transition metals are diluted magnetic semiconductors (DMS),[1,33] which attracted a lot of interest due to their potential applications in spintronics.[34] In this work, we fabricated Cu-doped ZnO nanostructures by a simple thermal evaporation method with mixed Zn and $CuCl_2$ powders as the source

* To whom correspondence should be addressed. E-mail: tomwu@ntu.edu.sg.
[†] Nanyang Technological University.
[‡] National University of Singapore.
[§] Institute of Materials Research and Engineering.

10.1021/jp710837h CCC: $40.75
Published on Web 06/07/2008

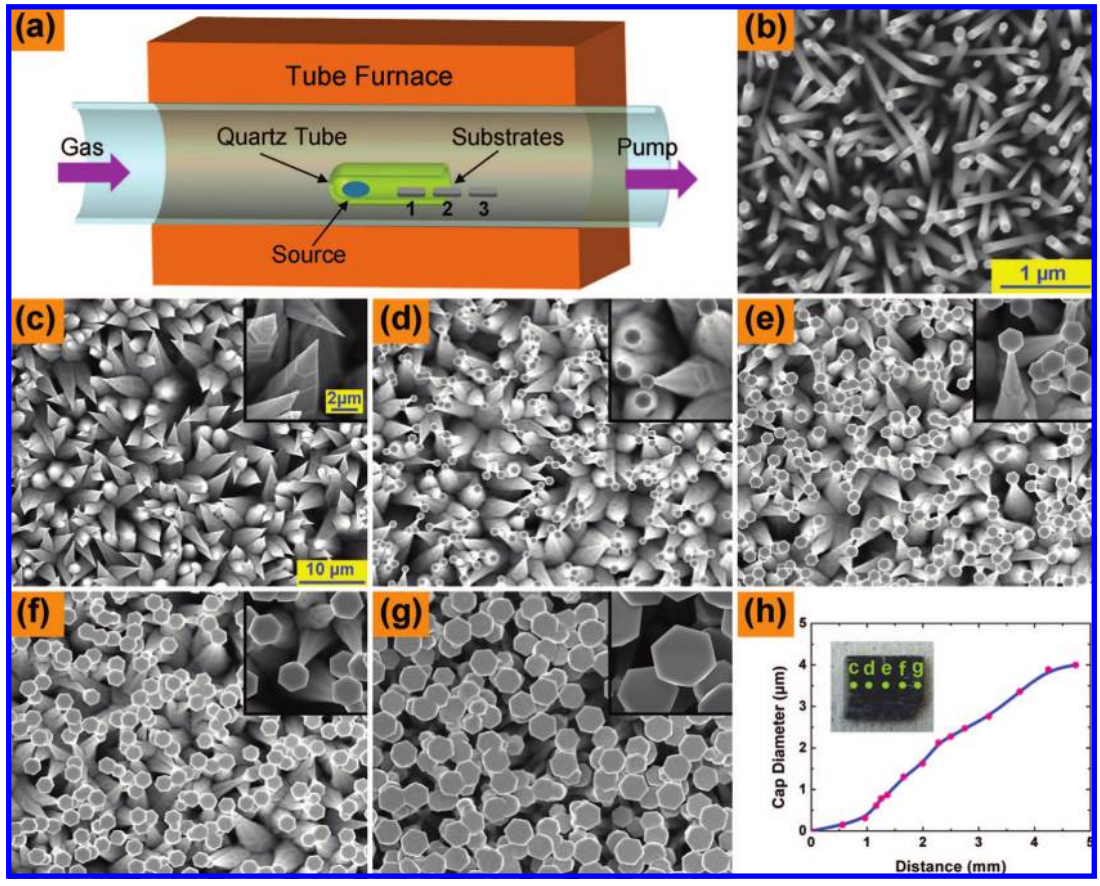

Figure 1. (a) A schematic drawing of the experimental setup. (b) A field-emission scanning electron microscopy (FESEM) image of pure ZnO nanowires grown without $CuCl_2$ in the source. (c−g) FESEM top views of Cu-doped ZnO nanostructures show a continuous morphological evolution between nanoneedles and nanonails in Cu-doped ZnO nanostructures. The five images have the same size. The insets show the closer views. The five insets have the same dimension. (h) The dependence of the cap diameter of nanonails on the distance from the left edge of substrate. The inset is a photograph of an actual sample with a dimension of ~8 mm × 5 mm. The locations of the SEM observations are highlighted.

material. PL measurements showed that Cu doping induces a red shift in both the sharp band edge and the broad green emissions. Room-temperature ferromagnetism (RTFM) was also detected in our samples.

Experimental Section

A schematic drawing of the experimental setup is shown in Figure 1a. Zn and $CuCl_2$ powders are chosen as source materials due to their low and approximate melting points (Zn 419 °C; $CuCl_2$ 620 °C). Zn powder (0.5 g) and $CuCl_2$ powder (0.1 g) were mixed carefully and ground for 30 minutes. The source powder was then inserted into the bottom of a slender one-end-sealed quartz tube with a diameter of 10 mm. The aim of this slender quartz tube is to concentrate the source vapor, which is critical for the formation of nanoneedles and nanonails. Before the nanowire growth, this slender quartz tube was put into the center area of a horizontal tube furnace (Lindberg/Blue Mini-Mite) with the opening facing the right. Carefully cleaned Si substrates were placed a few centimeters from the source on the right side, both inside and outside of the slender quartz tube. As we will show later, the location of the substrate appears to be an important factor determining the morphologies of the final products. 2-nm Au films were used as the catalyst and were predeposited on the substrates by sputtering. A carefully calibrated mass flow controller and meter was connected to the left end of the furnace tube. Argon mixed with 5% oxygen was used as the carrying gas with a controlled flow rate of 50 sccm (sccm denotes for standard cubic centimeter per minute). The pumping speed of a mechanical pump was regulated to maintain the pressure inside the quartz tube at 20 mbar during the evaporation. Typically, the temperature of the furnace was raised to 650 °C with a ramping rate of 50 °C/min and cooled down quickly to room temperature after 15 min of growth. Pure ZnO nanowire samples were fabricated through the same route (no $CuCl_2$ is used) for comparison. The as-fabricated Cu-doped samples show a light pink or red shade in addition to the dark gray color of the pure ZnO nanowire sample.

X-ray powder diffraction (XRD) patterns were recorded on a Bruker D8 Advanced diffractometer using Cu Kα radiation. SEM images were obtained on a JEOL JSM-6700F field emission scanning electron microscope. Transmission electron microscopy (TEM) images, selected area electron diffraction (SAED) patterns, and electron energy-dispersive spectrometer (EDX) were taken on a JEOL 2100 transmission electron microscope operating at 200 kV. The doping levels and the bonding characteristics were determined by X-ray photoelectron spectroscopy (XPS) using a VG ESCALAB 220i-XL system equipped with a monochromatic X-ray source. PL was studied at room temperature by using a continuous-wave He−Cd laser with a 325-nm line. Magnetization measurements were carried out using a superconducting quantum interference device (SQUID) magnetometer (Quantum Design, MPMSXL-5).

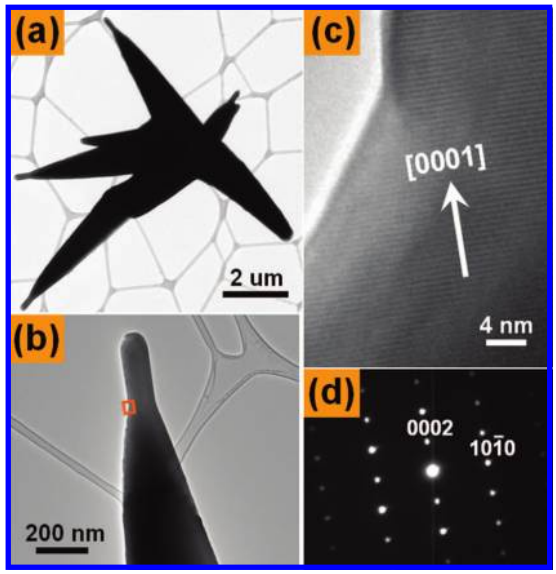

Figure 2. (a, b) Low-resolution TEM images of nanoneedles. A high-resolution image (c) and SAED pattern (d) were taken at the area specified in part b.

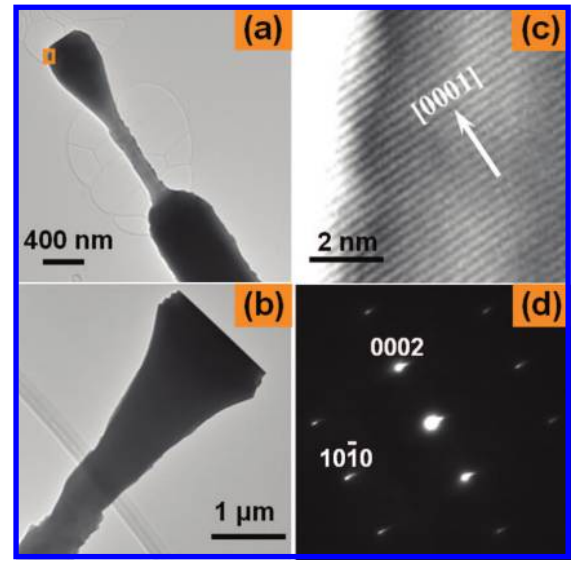

Figure 3. (a, b) Low-resolution TEM images of two nanonails. A high-resolution image (c) and SAED pattern (d) were taken at the area specified in part a.

Results and Discussion

Without $CuCl_2$ in the source, under the same experimental conditions, the pure ZnO samples always showed the commonly reported nanowire morphology (Figure 1b). On the other hand, the morphology of Cu-doped ZnO nanostructures exhibits a sensitive dependence on the locations of substrates. Nanoneedles were always found on the substrates located inside of the slender quartz tube (position 1 in Figure 1a), while nanonails often grow on the substrates put right outside of the tube (position 3 in Figure 1a). A gradual transition between these two morphologies was sometimes observed on the substrate put purposely on the rim of the slender tube (position 2 in Figure 1a). Parts c−g of Figure 1 show typical SEM images of the Cu-doped ZnO nanostructures with a continuous revolution from nanoneedles (Figure 1c) to nanonails (Figure 1g). The locations of the SEM observations are depicted on the photograph of the actual sample as shown in the inset of Figure 1h. All the nanostructures show good vertical alignment although the Si substrates are covered with amorphous silicon oxide. Figure 1h plots the cap sizes of the nanonails as a function of the distance from the left edge of the sample, which exhibits a monotonic increase. The diameter of the hexagonal caps can go from tens of nanometers up to several micrometers, while the sizes of conelike "body" and thin "neck" remain roughly unchanged. When the size of the nanonail caps increases beyond 5 μm, there is significant overlapping between the caps. In this situation, continuous films are effectively formed with porous structures underneath due to the much smaller dimensions of the necks. It is generally believed that formation mechanisms of nanonails and nanoneedles are very different due to their dramatically different morphologies. However, herein we demonstrated that a continuous transition from nanoneedles to nanonails can be reliably produced on a substrate with a size of only a few mm (the inset of Figure 1h). The morphologies of the nanostructures are unambiguously determined by the selection of source powder and the location of growth substrate.

ZnO has a wurtzite structure with a hexagonal unit cell (space group $P6_3mc$) and lattice parameters $a = 0.33$ and $c = 0.52$ nm.[1] In Figure 2, the TEM pictures of nanoneedles were taken on the samples shown in Figure 1c. The low resolution image (Figure 2a) indicates that the nanonails are connected at their bases. As shown in Figure 2b, the typical dimension of the small needles on top of the cones is ~100 nm. The high-resolution image (Figure 2c) indicates that the growth direction is [0001] with a coherent transition between the cone and the neck. The absence of visible defects, second phase, or precipitation means that the dopants are well-integrated into the lattice sites. The SAED pattern (Figure 2d) is consistent with the hexagonal wurtzite structure of ZnO with no second phase detected. Therefore, we can conclude that the Cu doping does not perturb significantly the lattice structure of the ZnO matrix.

The crystalline structure of nanonails was also studied by TEM. The low resolution TEM images of parts a and b of Figure 3 were taken on the samples shown in parts d and f of Figure 1, respectively. The top surfaces for both samples appear to be quite flat, consistent with the SEM observations. The roughness increases significantly in the neck and the cone areas underneath. Although the cap of the nanonails can reach several micrometers, the necks have much smaller dimensions of a few hundreds of nanometers. The high-resolution TEM image (Figure 3c) taken on the nanonail sample indicates that the growth direction is along [0001], the same as the nanoneedles. The SAED pattern (Figure 3d) of nanonails shows a good crystalline nature and is consistent with the high-resolution image.

XRD was used to study the crystal structures and the results are shown in Figure 4a. Only ZnO peaks were found in all the samples. Both the nanoneedles and the nanonails have the wurtzite structure. The absence of Cu, CuO, or Cu_2O peak excludes the existence of Cu-based clusters within the detection limit. The high intensity of the (002) peak suggests that [0001] is the preferred growth direction. As shown in Figure 4b, the (002) peaks of the doped sample show a clear shift of ~0.04° to the right compared to the pure ZnO nanowires, which agrees with previous studies.[35,36] The shrinkage of lattice constants after doping is due to the substitution of Zn^{2+} (0.06 nm) by smaller Cu^{2+} (0.057 nm).

A typical EDX spectrum of the nanoneedle sample is shown in Figure S1. From this spectrum we can only conclude that the absolute concentration of Cu in the nanostructures is lower than 4% due to the unknown contribution from the Cu TEM grids. To determine the precise Cu concentration, we carried

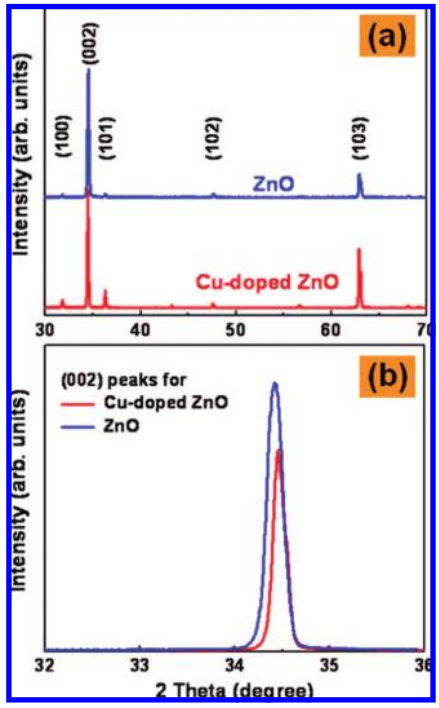

Figure 4. (a) XRD scans of the undoped and Cu-doped nanostructures. (b) The slow scans of the (002) peaks taken on these two samples.

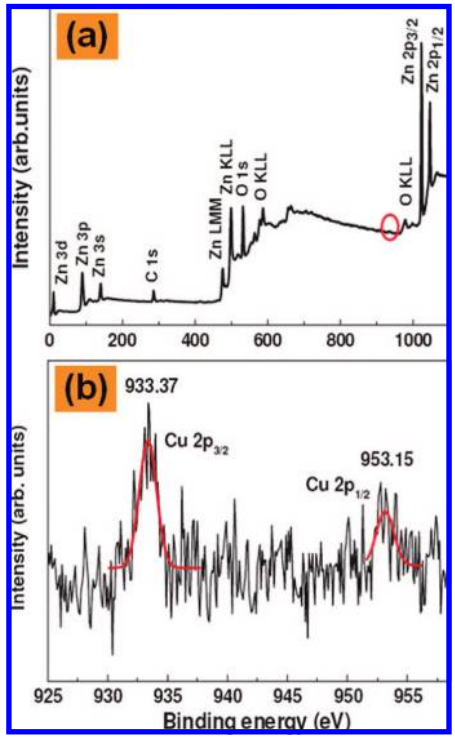

Figure 5. (a) The XPS survey spectrum of Cu-doped nanonails. (b) High-resolution scan of Cu $2p_{3/2}$ and $2p_{1/2}$ peaks.

out a XPS study on the nanonail sample. In the survey spectrum shown in Figure 5a, a very weak peak was detected at 933.37 eV. Its slow scan in Figure 5b shows Cu $2p_{3/2}$ peaks at 933.37 eV and Cu $2p_{1/2}$ at 953.15 eV. The quantitative analysis indicates that the Zn, Cu, and O concentrations are 52.90, 0.32, and 46.78%, respectively. We found that increasing the $CuCl_2$ ratio in the source does not lead to any significant increase of the Cu-doping level, indicating that either the solubility of Cu ions in ZnO is quite low[37,38] or transporting Cu from the source to the sample is inefficient. Therefore, in this report, we concentrate on the samples grown with 0.1 g of $CuCl_2$ for the structural, optical, and magnetic characterizations.

It is intriguing which and how the subtle variations of environmental conditions trigger the observed continuous morphological evolution between nanoneedles to nanonails. Controlling morphologies is very important because that the morphology of the nanostructures, as we will show later, strongly affects their luminescence properties. The growth of ZnO nanostructures often invokes not only one mechanism, but a convoluted combination of the VLS and VS processes. In a control experiment, we patterned the Au catalyst into patches using TEM grids and found that high-density ZnO nanostructures only grew on the areas covered with catalyst. Therefore, liquid-phase alloy droplets of Au appear to play an important role in the initial stage of growth by absorbing the incoming Zn vapor. Without the Au catalyst, the efficiency of forming nucleation sites on the smooth silicon substrates is quite low. However, unlike the conventional VLS growth, the liquid alloy droplets grow into islands with sizes much larger than the initial Au nanoparticles. This is in accordance with the fact that the base areas of the nanoneedles and nanonails show much larger dimensions than the size of Au nanoparticles. In the following stages of growth, the high Zn vapor pressure strongly promotes the VS growth. Therefore, the nanostructure growth in our experiments can be classified as a liquid-phase Au nanoparticles assisted VL process. The dominant fast VS growth often brings about novel self-assembled hierarchical structures, such as nanocombs and nanobridges.[39] Indeed, as shown in Figure 6a−f, we often observed comb-like structures with parallel nanonail or nanonail side branches (parts a and b of Figure 6), nanobrushes (Figure 6c), nanochains (Figure 6d), and nanoflowers (parts e and f of Figure 6).

To control the nanostructure morphology, it is very important to understand the factors that determine the growth speeds along various orientations and their relative ratios. The wurtzite structure of ZnO exhibits polar-terminated (0001) and nonpolar low-symmetry $(10\bar{1}0)$ faces. It is well-known that in most situations the growth rates of the different family of planes follow the sequence $(0001) > (10\bar{1}1) > (10\bar{1}0)$.[40] There are several reasons why the (0001) plane shows the highest growth speed, promoting the one-dimensional growth. One is that the Zn (0001) plane has the lowest surface energy, which tends to be the most stable to resist oxidation.[23] Since the temperature of the growth zone is above the Zn melting temperature, this liquid-phase growth front is highly effective to absorb the incoming Zn vapor and maintains a high growth speed. Another factor is that the top areas of nanowires always receive a high flux of Zn vapor than the shaft due to the shadow effect intrinsic to all physical vapor processes.[41] If the growth along the [0001] direction dominates, then nanowires often grow continuously with homogeneous diameters.

However, under certain environmental conditions, other structures like nanoneedles are preferred. In some aspects, the morphological change between nanowires and nanoneedles resembles the transition from a layer-to-layer (2D) mode to a three-dimensional (3D) mode in the thin film growth.[42,43] A flux of vapor particles and surface diffusion of adatoms after adsorption play dominant roles in both processes. In the thin film growth, with negligible surface desorption, the height h describing the local position of the moving surface at $\vec{r}$ obeys a conservation law,[44]

$$\partial_t h(\vec{r}, t) = -\vec{\nabla} \cdot \vec{j}[\nabla h(\vec{r}, t)] + \eta(\vec{r}, t) \quad (1)$$

where $\vec{j}$ is the surface diffusion current, η represents the

fluctuation of the incoming flux. $\vec{j}$ determines the growth morphology and is curtailed by the Ehrlich−Schwoebel barrier (ESB).[45,46] ESB is a result of the lower atom coordination and the localized nature of the dangling bonds at step edges. During growth, ESB limits the mass diffusion across step edges, which could occur when the atoms move either down from an island or between different facets. The formation of nanoneedles strongly indicates the existence of ESB for the diffusion of adatoms on the ZnO (0001) top surface, that is, the growth front. If ESB is negligibly small and the surface diffusion is not constrained, then the shape of growth products is mainly determined by the crystalline-plane-specific surface energies, and nanowires often form as a result. Otherwise, the island nucleation competes against the surface diffusion, preventing the ideal layer-by-layer growth on the top surface. The effect of ESB combining with the continuous supply of Zn vapor impinging on the surface basically determines the slop, that is, the sharpness of the nanoneedles.

In our experiments, the source vapor pressures are among the critical factors determining the size of ESB and the ensuing nanostructure morphologies. The use of $CuCl_2$ is critical for the formation of nanoneedles and nanonails. Without it, only ZnO nanowires can be obtained (Figure 1b). We note here that, besides $CuCl_2$, other rare earth metal chlorides can also trigger the growth of nanoneedles and nanonails. As shown in Figure S2 of the Supporting Information, our preliminary results suggest that nanostructures with similar morphologies can also be grown with mixed Zn and $MnCl_2$ powders. It is well-known that the growth of ZnO nanostructures is very sensitive to the compositional change of the source vapor. For example, several previous reports suggested that a trace amount of In vapor can dramatically increase the evaporation rate[41] and even cause the structural change from [0001] axial nanowires to [11$\bar{2}$0] axial nanobelts.[47] In our experiments, $CuCl_2$ decomposes into Cu and Cl_2 vapors (Figure S3), which might selectively modify the growth speeds of various ZnO facets. Similar to the epitaxial thin film growth,[43,48] these vapors may also act as surfactants, modifying ESB and the mobility of adatoms. If Cu and Cl_2 absorb preferably on the edge of the growth front, then the subsequent layer grown on top will achieve a slightly smaller dimension, which eventually yields a needlelike morphology.

The SEM and TEM studies indicate that the stems of the nanoneedles and nanonails have very similar conelike morphologies. Therefore, the growth of the hexagonal tops on nanonails must occur at the last stage of the growth process. This scenario is consistent with our proposed model for the nanoneedle growth in the sense that the termination of the Cu and Cl_2 vapors near the end of evaporation changes the mode of growth. The observed nanonails are similar to the undoped products reported previously.[39,41,49] There are at least two factors promoting the formation of nanonails. One is that the top surfaces of nanonails always receive more incoming source vapor than the stems underneath due to the shadow effect.[41] This trend further accelerates as the caps of the nanonails grow bigger. The other factor is the abrupt increase of the O/Zn ratio as the Zn vapor runs out near the end of evaporation. This change may significantly boost the lateral growth along the [10$\bar{1}$0] direction and promotes the formation of caps on the necks of nanoneedles.[49] In the future, further studies on the effects of environmental factors such as the growth time, the flow rate, the concentration of carrying gas, and the $Zn/CuCl_2$ ratio are needed to elicit the growth mechanism and to achieve a precise control of the nanostructure morphology.

One natural consequence of the above proposed mechanism is that the nanoneedles should show much higher densities of defects and oxygen vacancies than the nanonails. In agreement with previous reports on ZnO towers,[50,51] the inset of Figure 1c shows a high density of defects on the nanoneedle surfaces. In contrast, the top surfaces of nanonails (parts d−g of Figure 1 and parts a and b of Figure 3) appear to be very smooth and are free from imperfections. Additionally, the nanonail samples are always located outside of the slender quartz tube and are exposed to a continuous supply of oxygen. The ratio of oxygen/zinc becomes much higher as the source vapor is running out at the last stage of growth. Therefore, more oxygen is incorporated during the formation of nanonail caps. It is well-

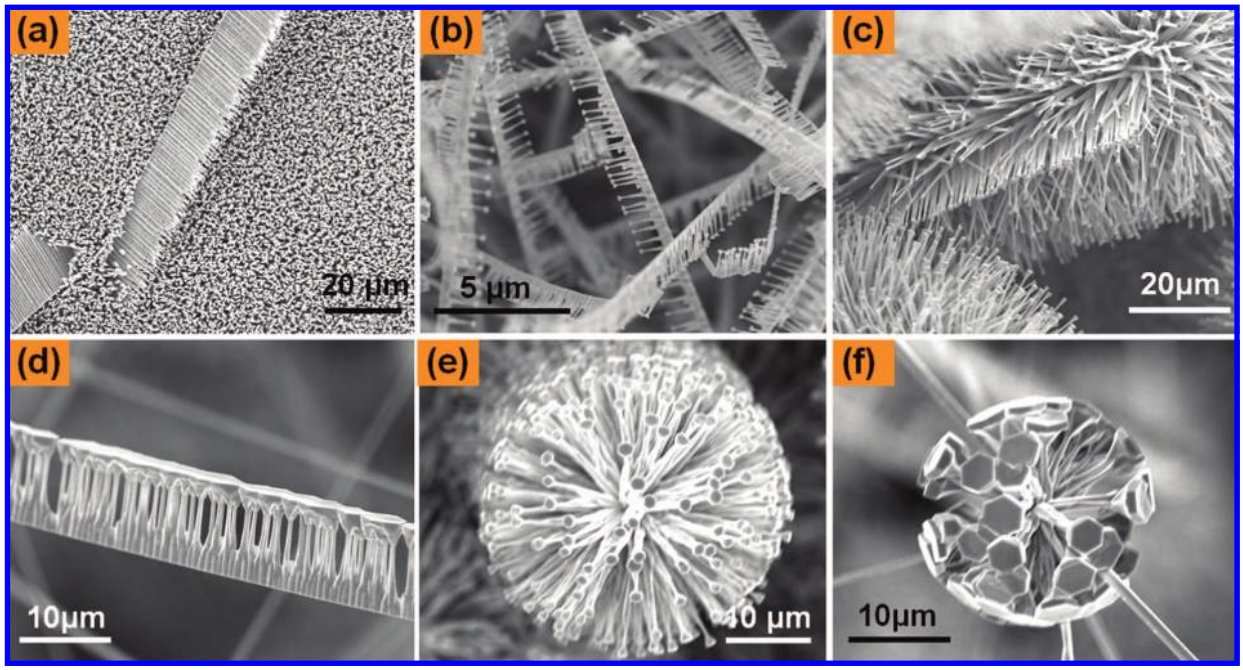

Figure 6. SEM images of self-assembled Cu-doped ZnO nanostructures. Nanocombs with side branches of nanoneedles (a) or nanonails (b). (c) Nanobrushes with a high density of side branches. (d) A nanochain composed of connected nanonails. Nanoflowers composed of many nanonails with small caps (e) or large caps (f).

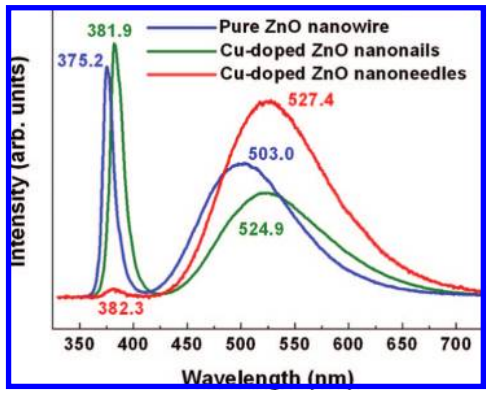

Figure 7. Room-temperature PL spectra of pure ZnO nanowire, Cu-doped ZnO nanonails, and nanoneedles.

known that the densities of defects and oxygen vacancies affect significantly the physical properties of oxide nanostructures. This correlation between structure and property was verified by the PL study. Figure 7 shows room temperature PL spectra of the pure ZnO nanowires, the Cu-doped ZnO nanoneedles, and nanonails. All the samples show two distinct emission peaks: a sharp one in the UV region and another broad one in the visible green region. The UV peak corresponds to the ZnO band gap, and the green peak is commonly related to singly ionized oxygen vacancies and defects.[31,52,53] The UV peaks of undoped ZnO nanowires, doped nanonails, and nanoneedles are located at 375.2, 381.9, and 382.3 nm, respectively. This red shift of ~7 nm in the Cu-doped samples indicates a reduction of ZnO band gap caused by the Cu doping. A similar red shift of the UV peak and a band-edge modification were also observed by He et al. in Ni-doped ZnO nanowires.[27] This reduction of the band gap with Cu doping also indicates that Cu ions substitute for the Zn sites in ZnO.[54] Interestingly, the intensity of the UV peak of the nanonail sample is comparable to that of the pure ZnO nanowire sample, while the nanoneedle sample shows a much lower intensity of the band gap emission than that of the other two samples. The dominance of the green emission in the nanoneedle sample indicates that it exhibits a much higher defect concentration than the nanonails. Since the nanoneedles are just nanonails without caps, we can conclude that the defect distribution in nanonail structures is not homogeneous. There is a much higher concentration of defects on the body surface than on the cap, which is consistent with the SEM and TEM observations.

Recently, there have been intensive interests in studying ZnO-based DMS due to their potential applications in spintronics. However, it is still controversial whether RTFM observed in these ZnO-based materials is intrinsic or due to the unintentional formation of magnetic metal clusters.[33] In this sense, studying Cu doping is of vital importance since neither Cu nor Cu-based oxides show strong ferromagnetism. Furthermore, the substitution of Zn by Cu is a p-type doping, which may promote RTFM.[55] Density functional calculations also predicted half-metallic ferromagnetism in Cu-doped ZnO without any clustering tendency of the Cu atoms.[55] Recently, both RTFM and anomalous Hall effect were observed in Cu-doped ZnO thin films.[36,56,57] Herng et al. also reported RTFM and magnetic anisotropy in Cu-doped ZnO nanoneedles.[35] However, there have been no report on the magnetic properties of transition-metal-doped ZnO nanonails. Figure 8a shows typical $M-H$ curves of a Cu-doped nanonail sample taken at both 5 and 300 K. The observed hysteresis loops indicate the existence of ferromagnetism at both temperatures, consistent with previous

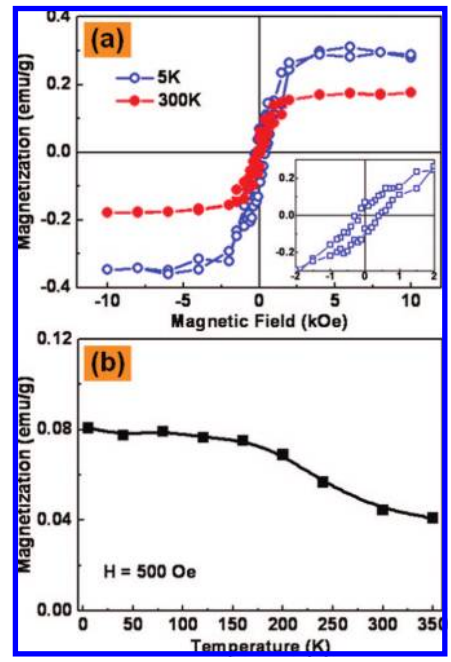

Figure 8. (a) Magnetization-field ($M-H$) loops of a Cu-doped ZnO nanonail sample taken at 5 and 300 K. The inset shows the $M-H$ loop of the 5 K data in the low-field regime. (b) Magnetization as a function of temperature for the same sample.

studies.[35,36,56] Temperature-dependent magnetization ($M-T$) curve indicates that the FM transition temperature is higher than room temperature, in accordance with the other reports.[56,57] The low Cu doping concentration does not favor the conventional superexchange or double exchange mechanism as the origin of the observed RTFM. On the other hand, oxygen vacancies and surface defects could play very important roles in enhancing the magnetism. Our XPS, SEM, and PL data indicate that there are substantial oxygen vacancies and surface defects in the Cu-doped ZnO samples. It has been shown that in clusters of oxygen vacancies, the Hund's coupling energy exceeds the separation between the hybridized orbital levels, giving rise to a net magnetic moment.[58] Similarly, Durst et al. argued that defects tend to form bound magnetic polarons that stabilize the ferromagnetic ordering. The enhancement of RTFM by structural defects has also been observed in transition-metal-doped thin films and nanocrystals.[59,60] Further studies using SQUID, TEM, and magnetic circular dichroism are needed to determine unambiguously the origin of the observed RTFM.

Conclusions

In summary, Cu-doped ZnO nanoneedles and nanonails were synthesized by thermally evaporating Zn and $CuCl_2$ powders. We observed a continuous morphological evolution between nanoneedles and nanonails with a high tenability and reproducibility. This chloride-based thermal evaporation method appears to be a general approach to fabricate transition-metal-doped ZnO nanomaterials with novel morphologies. Such a controlled doping has extensive implications and affects the crystalline and electronic structures of ZnO. In our experiments, the Cu doping results in a decrease in the lattice parameter and a red shift of the energy band edge. The strong correlation between morphologies and optical properties was illustrated in the significantly different luminescence properties of nanoneedles and nanonails. Finally, RTFM was detected in Cu-doped ZnO nanostructures, which may find novel applications in spintronic devices.

Supporting Information Available: A typical EDX spectrum of the nanoneedle sample, SEM pictures of Mn-doped ZnO nanoneedles and nanonails, decomposition of $CuCl_2$ at the growth temperature. This information is available free of charge via the Internet at http://pubs.acs.org.

Acknowledgment. We acknowledge research Grant SUG 20/06 and Institute of Materials Research and Engineering for support.

References and Notes

(1) Ozgur, U.; Alivov, Y. I.; Liu, C.; Teke, A.; Reshchikov, M. A.; Dogan, S.; Avrutin, V.; Cho, S. J.; Morkoc, H. *J. Appl. Phys.* **2005**, *98*, 041301.
(2) Hara, K.; Horiguchi, T.; Kinoshita, T.; Sayama, K.; Sugihara, H.; Arakawa, H. *Sol. Energy Mater. Sol. Cells* **2000**, *64*, 115.
(3) Heiland, G. *Sens. Actuators* **1982**, *2*, 343.
(4) Yumoto, H.; Inoue, T.; Li, S. J.; Sako, T.; Nishiyama, K. *Thin Solid Films* **1999**, *345*, 38.
(5) Carcia, P. F.; McLean, R. S.; Reilly, M. H.; Nunes, G. *Appl. Phys. Lett.* **2003**, *82*, 1117.
(6) Chopra, K. L.; Major, S.; Pandya, D. K. *Thin Solid Films* **1983**, *102*, 1.
(7) Wang, Z. L. *J. Phys.: Condens. Matter* **2004**, *16*, R829.
(8) Ng, H. T.; Han, J.; Yamada, T.; Nguyen, P.; Chen, Y. P.; Meyyappan, M. *Nano Lett.* **2004**, *4*, 1247.
(9) Soci, C.; Zhang, A.; Xiang, B.; Dayeh, S. A.; Aplin, D. P. R.; Park, J.; Bao, X. Y.; Lo, Y. H.; Wang, D. *Nano Lett.* **2007**, *7*, 1003.
(10) Li, Q. H.; Liang, Y. X.; Wan, Q.; Wang, T. H. *Appl. Phys. Lett.* **2004**, *85*, 6389.
(11) Lee, C. J.; Lee, T. J.; Lyu, S. C.; Zhang, Y.; Ruh, H.; Lee, H. J. *Appl. Phys. Lett.* **2002**, *81*, 3648.
(12) Huang, M. H.; Mao, S.; Feick, H.; Yan, H.; Wu, Y.; Kind, H.; Weber, E.; Russo, R.; Yang, P. *Science* **2001**, *292*, 1897.
(13) Wang, X. D.; Song, J. H.; Liu, J.; Wang, Z. L. *Science* **2007**, *316*, 102.
(14) Zheng, M. J.; Zhang, L. D.; Li, G. H.; Shen, W. Z. *Chem. Phys. Lett.* **2002**, *363*, 123.
(15) Huang, M. H.; Wu, Y.; Feick, H.; Tran, N.; Weber, E.; Yang, P. *Adv. Mater.* **2001**, *13*, 113.
(16) Wager, R. S.; Ellis, W. C. *Appl. Phys. Lett.* **1964**, *4*, 89.
(17) Yao, B. D.; Chan, Y. F.; Wang, N. *Appl. Phys. Lett.* **2002**, *81*, 757.
(18) Sears, G. W. *Acta Metal.* **1955**, *3*, 367.
(19) Sears, G. W. *Acta Metal.* **1955**, *3*, 361.
(20) Kong, X. Y.; Wang, Z. L. *Nano Lett.* **2003**, *3*, 1625.
(21) Pan, Z. W.; Dai, Z. R.; Wang, Z. L. *Science* **2001**, *291*, 1947.
(22) Zhang, B. P.; Binh, N. T.; Wakatsuki, K.; Segawa, Y.; Yamada, Y.; Usami, N.; Kawasaki, M.; Koinuma, H. *Appl. Phys. Lett.* **2004**, *84*, 4098.
(23) Gao, P. X.; Lao, C. S.; Ding, Y.; Wang, Z. L. *Adv. Funct. Mater.* **2006**, *16*, 53.
(24) Yuhas, B. D.; Zitoun, D. O.; Pauzauskie, P. J.; He, R.; Yang, P. *Angew. Chem., Int. Ed.* **2006**, *45*, 420.
(25) Cho, Y. M.; Choo, W. K.; Kim, H.; Kim, D. *Appl. Phys. Lett.* **2002**, *80*, 3358.
(26) Chang, Y. Q.; Wang, D. B.; Luo, X. H.; Xu, X. Y.; Chen, X. H.; Li, L.; Chen, C. P.; Wang, R. M.; Xu, J.; Yu, D. P. *Appl. Phys. Lett.* **2003**, *83*, 4020.
(27) He, J. H.; Lao, C. S.; Chen, L. J.; Davidovic, D.; Wang, Z. L. *J. Am. Chem. Soc.* **2005**, *127*, 16377.
(28) Ronning, C.; Gao, P. X.; Ding, Y.; Wang, Z. L.; Schwen, D. *Appl. Phys. Lett.* **2004**, *84*, 783.
(29) Liu, J. J.; Yu, M. H.; Zhou, W. L. *Appl. Phys. Lett.* **2005**, *87*, 172505.
(30) Liu, L. Q.; Xiang, B.; Zhang, X. Z.; Zhang, Y.; Yu, D. P. *Appl. Phys. Lett.* **2006**, *88*, 063104.
(31) Garces, N. Y.; Wang, L.; Bai, L.; Giles, N. C.; Halliburton, L. E.; Cantwell, G. *Appl. Phys. Lett.* **2002**, *81*, 622.
(32) Kanai, Y. *Jpn. J. Appl. Phys.* **1991**, *30*, 703.
(33) Janisch, R.; Gopal, P.; Spaldin, N. A. *J. Phys.: Condens. Matter* **2005**, *17*, R657.
(34) Wolf, S. A.; Awschalom, D. D.; Buhrman, R. A.; Daughton, J. M.; von Molnar, S.; Roukes, M. L.; Chtchelkanova, A. Y.; Treger, D. M. *Science* **2001**, *294*, 1488.
(35) Herng, T. S.; Lau, S. P.; Yu, S. F.; Yang, H. Y.; Wang, L.; Tanemura, M.; Chen, J. S. *Appl. Phys. Lett.* **2007**, *90*, 032509.
(36) Chakraborti, D.; Narayan, J.; Prater, J. T. *Appl. Phys. Lett.* **2007**, *90*, 062504.
(37) Park, M. S.; Min, B. I. *Phys. Rev. B* **2003**, *68*, 224436.
(38) Wang, X. F.; Xu, J. B.; Cheung, W. Y.; An, J.; Ke, N. *Appl. Phys. Lett.* **2007**, *90*, 212502.
(39) Shen, G. Z.; Bando, Y.; Chen, D.; Liu, B. D.; Zhi, C. Y.; Golberg, D. *J. Phys. Chem. B* **2006**, *110*, 3973.
(40) Laudise, R. A.; Ballman, A. A. *J. Phys. Chem.* **1960**, *64*, 688.
(41) Lao, J. Y.; Huang, J. Y.; Wang, D. Z.; Ren, Z. F. *Nano Lett.* **2003**, *3*, 235.
(42) Villain, J. *J. Phys. I* **1991**, *1*, 19.
(43) Tersoff, J.; Vandergon, A. W. D.; Tromp, R. M. *Phys. Rev. Lett.* **1994**, *72*, 266.
(44) Siegert, M.; Plischke, M. *Phys. Rev. Lett.* **1994**, *73*, 1517.
(45) Ehrlich, G.; Hudda, F. G. *J. Chem. Phys.* **1966**, *44*, 1039.
(46) Schwoebel, R. *J. Appl. Phys.* **1969**, *40*, 614.
(47) Fan, H. J.; Barnard, A. S.; Zacharias, M. *Appl. Phys. Lett.* **2007**, *90*, 143116.
(48) Vrijmoeth, J.; Vandervegt, H. A.; Meyer, J. A.; Vlieg, E.; Behm, R. J. *Phys. Rev. Lett.* **1994**, *72*, 3843.
(49) Shen, G. Z.; Bando, Y.; Liu, B. D.; Golberg, D.; Lee, C.-J. *Adv. Funct. Mater.* **2006**, *16*, 410.
(50) Tong, Y. H.; Liu, Y. C.; Shao, C. L.; Mu, R. X. *Appl. Phys. Lett.* **2006**, *88*, 123111.
(51) Wang, F. F.; Cao, L.; Pan, A. L.; Liu, R. B.; Wang, X.; Zhu, X.; Wang, S. Q.; Zou, B. S. *J. Phys. Chem. C* **2007**, *111*, 7655.
(52) Vanheusden, K.; Warren, W. L.; Seager, C. H.; Tallant, D. R.; Voigt, J. A.; Gnade, B. E. *J. Appl. Phys.* **1996**, *79*, 7983.
(53) Xu, C. X.; Sun, X. W.; Zhang, X. H.; Ke, L.; Chua, S. J. *Nanotechnology* **2004**, *15*, 856.
(54) Lee, H. J.; Kim, B. S.; Cho, C. R.; Jeong, S. Y. *Phys. Status Solidi B* **2004**, *241*, 1533.
(55) Ye, L.-H.; Freeman, A. J.; Delley, B. *Phys. Rev. B* **2006**, *73*, 033203.
(56) Hou, D. L.; Ye, X. J.; Meng, H. J.; Zhou, H. J.; Li, X. L.; Zhen, C. M.; Tang, G. D. *Appl. Phys. Lett.* **2007**, *90*, 142502.
(57) Buchholz, D. B.; Chang, R. P. H.; Song, J. H.; Ketterson, J. B. *Appl. Phys. Lett.* **2005**, *87*, 082504.
(58) Banerjee, S.; Mandal, M.; Gayathri, N.; Sardar, M. *Appl. Phys. Lett.* **2007**, *91*, 182501.
(59) Kaspar, T. C.; Heald, S. M.; Wang, C. M.; Bryan, J. D.; Droubay, T.; Shutthanandan, V.; Thevuthasan, S.; McCready, D. E.; Kellock, A. J.; Gamelin, D. R.; Chambers, S. A. *Phys. Rev. Lett.* **2005**, *95*, 217203.
(60) Radovanovic, P. V.; Gamelin, D. R. *Phys. Rev. Lett.* **2003**, *91*, 157202.

JP710837H